*inorganics*

MDPI

*Article*

# Photocatalytic Activity of Multicompound $TiO_2/SiO_2$ Nanoparticles

**Filipp Temerov [1], Janne Haapanen [2], Jyrki M. Mäkelä [2] and Jarkko J. Saarinen [1,*]**

[1] Department of Chemistry, University of Eastern Finland, P.O. Box 111, FI-80101 Joensuu, Finland; filipp.temerov@uef.fi
[2] Aerosol Physics Laboratory, Department of Physics, Tampere University, P.O. Box 692, FI-33101 Tampere, Finland; janne.haapanen@tuni.fi (J.H.); jyrki.makela@tuni.fi (J.M.M.)
* Correspondence: jarkko.j.saarinen@uef.fi

**Abstract:** Multicompound $TiO_2/SiO_2$ nanoparticles with a diameter of 50–70 nm were generated using a liquid flame spray (LFS) nanoparticle deposition in a single flame. Here, we study the photocatalytic activity of deposited multicompound nanoparticles in gas-phase via oxidation of acetylene into carbon dioxide that gives new insight about the multicompound nanoparticle morphology. A small addition of $SiO_2$ content of 0.5%, 1.0% and 3.0% significantly suppressed the photocatalytic activity by 33%, 44% and 70%, respectively, whereas 5.0% $SiO_2$ addition completely removed the activity. This may be due to a formation of a thin passivating $SiO_2$ layer on top of the of the $TiO_2$ nanostructures during the LFS nanoparticle deposition. Surface wetting results support this hypothesis with a significant increase in water contact angle as the $SiO_2$ content is increased.

**Keywords:** photocatalysis; $TiO_2$; $SiO_2$; nanoparticles; liquid flame spray (LFS)



**Citation:** Temerov, F.; Haapanen, J.; Mäkelä, J.M.; Saarinen, J.J. Photocatalytic Activity of Multicompound $TiO_2/SiO_2$ Nanoparticles. *Inorganics* **2021**, *9*, 21. https://doi.org/10.3390/inorganics9040021

Academic Editor: Gianfranco Pacchioni

Received: 23 February 2021
Accepted: 21 March 2021
Published: 25 March 2021



## 1. Introduction

Accumulation of toxic compounds into ecosystem is a global and growing problem. Effective catalytic materials are needed to remove toxic, typically organic, compounds from wastewater to airborne pollution. Several technologies have been developed for solving this problem ranging from advanced oxidative technologies (AOT) [1] widely used in the wastewater management plants to solar-driven catalysis using novel multicompound metal and metal oxide based photocatalysts [2]. Photocatalysis is a promising approach for heterogeneous catalysis in which chemical reactions can be accelerated by the excitation of a catalyst by incident photons. The photocatalytic activity depends on the ability of the photocatalyst to form electron-hole pairs, which produce free radicals, which participate in secondary reactions [2].

Nowadays the most studied photocatalyst is titanium dioxide ($TiO_2$). $TiO_2$ is a well-known, non-toxic and widely used white pigment with good photostability [3]. In anatase crystalline form the bandgap between the valence and the conduction band is 3.2 eV that corresponds to a photon wavelength of 387 nm in the ultraviolet A (UVA) range. Photons with shorter wavelength (and thus higher energy) can excite electrons from the valence band to the conduction band: the generated electrons and holes can diffuse onto the surface and facilitate various reduction and oxidation reactions, respectively. In the seminal work by Fujishima and Honda in 1972 [4], water splitting to hydrogen and oxygen was demonstrated by irradiating $TiO_2$ electrode with UVA light in a photochemical cell. The photocatalytic activity of $TiO_2$ has been widely investigated ranging from controlled wettability of surfaces to selective conversion of $CO_2$ into fuels ($CH_4$, $CH_3OH$, HCHO and HCOOH) [5] $TiO_2$ nanostructures can also be used to generate hydrogen from water [6] and decomposition of organic molecules (pollutants) [7]. Additionally, the photocatalytic activity of $TiO_2$ can be modified by doping $TiO_2$ nanostructures with metals and non-metals [8–10].

There exists also a large variety of $TiO_2$ based photocatalysts such as $TiO_2/SiO_2$, $Al_2O_3$-$TiO_2$ and $TiO_2$-zeolite. Introduction of additional elements in $TiO_2$ system can enhance the photocatalytic activity. For example, 2% $Al_2O_3$-$TiO_2$ nanocomposite [11] for selective degradation of imazapyr showed a two- to three-fold improvement of photocatalytic activity compared to mesoporous $TiO_2$, whereas $TiO_2$-zeolite photocatalysts from metakaolin and rice husk ash [12] showed an enhanced photoactivity compared to powder $TiO_2$. Alternatively, $TiO_2/SiO_2$/graphene oxide (GO) photocatalyst [13] demonstrated enhanced visible light photoactivity for self-cleaning surfaces resulting from synergetic action of $TiO_2$ and GO in which $TiO_2$ produces electron-hole pairs and GO quickly transfer them to the surface for redox reactions. Many reports have been devoted to doping $TiO_2$ doping with $SiO_2$ such as $TiO_2/SiO_2$ nanocomposite [14,15] for efficient removal of organic pollutants. However, a reduced photocatalytic response of $TiO_2/SiO_2$ system [16] has also been observed since $SiO_2$ can form blocking layer on top of $TiO_2$ nanoparticles preventing electron and hole transport onto the nanoparticle surface.

In this paper we use a liquid flame spray (LFS) nanoparticle deposition that is versatile tool for depositing a large range of metal and metal oxide nanoparticles on various substrates [17,18]. The LFS process contains a high velocity and high temperature hydrogen-oxygen flame in which an organometallic precursor is fed. The precursor evaporates, nucleates and forms solid nanoparticles that can be collected on various substrates. The LFS process parameters such as gas flows, precursor feed rate and burner to substrate distance can easily be modified for a deposition of nanoparticles with highly controlled size and amount. Typically, the LFS deposition produces a highly porous network of interconnected nanoparticles with porosity up to 95% [19].

LFS deposited $TiO_2$ nanoparticles are well suitable for photocatalysis. We have previously utilized LFS nanoparticle deposition for photocatalytic wettability conversion of $TiO_2$ nanoparticle coated paperboard [20]. A detailed surface chemical analysis was carried out using both X-ray photoelectron spectroscopy [21] and time-of-flight secondary ion mass spectroscopy [22] that confirmed the role of hydrocarbons and hydroxyl groups generated on the surface via photocatalytic activation. The LFS deposited nanoparticles adhere onto the surface via rather weak van der Waals forces and, therefore, the LFS deposited nanoparticles can easily be removed by wear as has been shown earlier [23]. Multicompound nanomaterials can also be generated using LFS and Teisala et al. [24] showed that LFS generated binary particles sinter better when mixing some amount of $SiO_2$ into $TiO_2$. They showed that even a small fraction of $SiO_2$ will make the LFS deposited $TiO_2$ nanoparticles more stable, i.e., having more wear resistance. The reason for this is that the $SiO_2$ helps particle sintering (neck-forming) or, alternatively, the $SiO_2$ can coat or cover the $TiO_2$ nanoparticles and, thus, support the deposited structure.

Traditionally photocatalytical activity has been characterized using an indirect method based on a color transformation of an optical dye, such as methylene blue (MB) [25]. However, such an indirect method should not be used for photocatalytic activity measurements; this is especially true at visible wavelengths as the incident light itself can bleach the used dye and, therefore, induce an erroneous result [26]. Moreover, during the sample immersion in water solution nanoparticles may detach and migrate from substrate into the solution. Therefore, a much better alternative to measure photocatalytic activity is based on a gas-phase oxidation of small organic compounds such (e.g., methane, acetylene) due to their relatively simple structures which can be easily broken. The mineralization of carbon compounds into $CO_2$ can be directly and simply measured by monitoring the rate of $CO_2$ increase in the reaction chamber. Moreover, the gas-phase detection removes all mechanical stresses induced by liquid phase methods on the nanostructures.

In this work, we report a simple fabrication method for deposition of $TiO_2/SiO_2$ multicompound nanoparticles in a single flame. The photocatalytic activity was characterized using an in-house built photoreactor based on decomposition of acetylene into $CO_2$ [27,28]. The multicompound nanoparticles showed a small increase in the adhesion but increase of $SiO_2$ content even up to 5% completely reduced the photocatalytic activity. The observed

reduction of photocatalytic activity may be associated to a formation of a thin passivating layer on top of photocatalytically active $TiO_2$ that prevents the diffusion of the generated electrons and holes onto the surface. A thin passivating layer is also supported by the observed water contact angles that are significantly increased in the presence of $SiO_2$.

## 2. Results and Discussion

Five photocatalysts were produced by the LFS method with different $TiO_2$ and $SiO_2$ content (pure $TiO_2$ and $TiO_2/SiO_2$ with ratios of 99.5/0.5, 99.0/1.0, 97.0/3.0 and 95.0/5.0, respectively). Surface morphology of all LFS nanoparticle deposited samples were analyzed by using scanning electron microscopy (SEM). Figure 1 displays the distribution of nanoparticles that is rather uniform for all depositions. Average nanoparticle diameter ranged from 40 nm to 80 nm with majority of particles within 50–70 nm range independent of the used precursor formulation that is in good agreement with our previous studies with similar LFS deposition parameters [20,21].

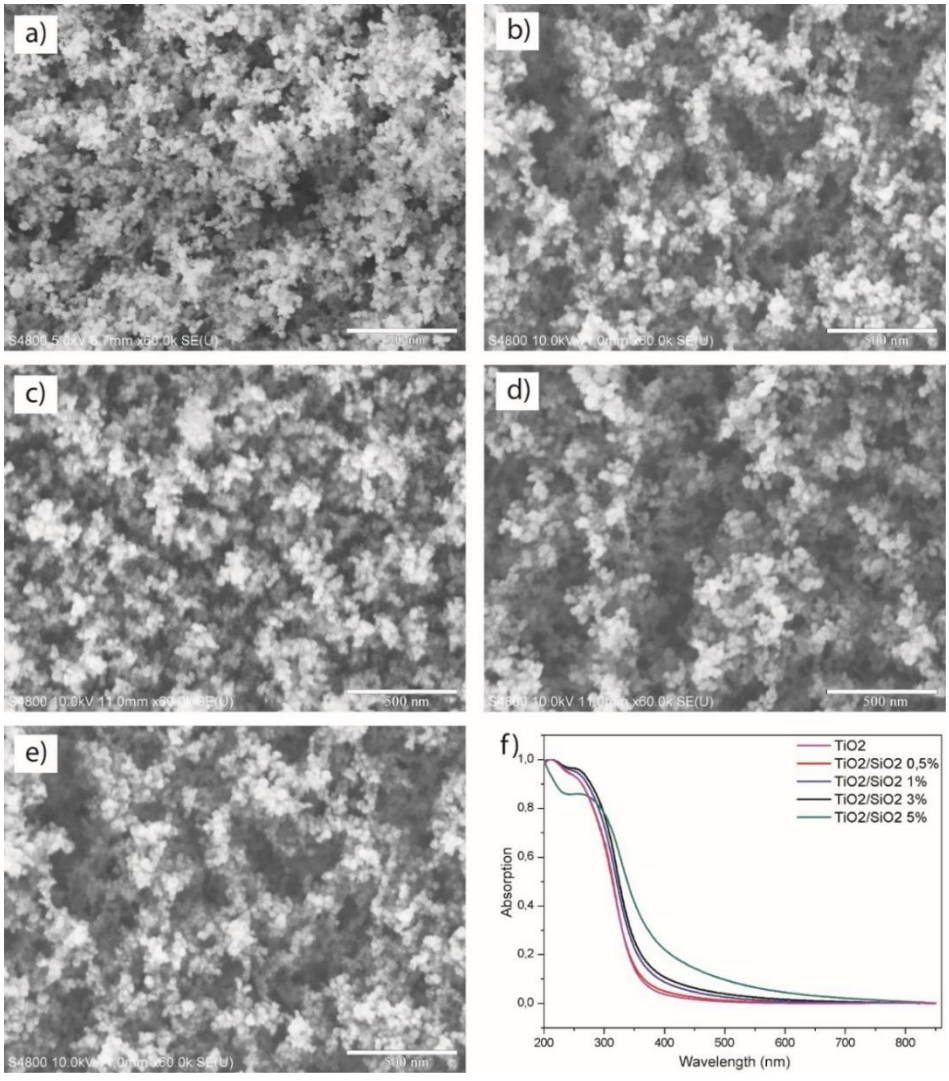


**Figure 1.** SEM images of (**a**) $TiO_2$, (**b**) $TiO_2/SiO_2$ 99.5/0.5, (**c**) $TiO_2/SiO_2$ 99.0/1.0, (**d**) $TiO_2/SiO_2$ 97.0/3.0, (**e**) $TiO_2/SiO_2$ 95.0/5.0 and (**f**) UV-Vis absorption spectra of the corresponding samples.

It can be concluded from Figure 1 that is difficult to see any significant effects in morphology caused by variation in the $TiO_2/SiO_2$ content. A small increase in the nanoparticle diameter (to 70–80 nm) with an increased aggregation tendency can be seen with increased $SiO_2$ content. Figure 1f shows UV-Vis absorption spectrum of the samples. Increased $SiO_2$

content is followed by a reduced $TiO_2$ absorption in wavelength range of 200–300 nm. This is expected as $SiO_2$ has a significantly lower absorption in the UV region compared to $TiO_2$ and, thus, increased $SiO_2$ content will reduce UV absorption of the multicompound nanostructures.

To study the actual particle formation photocatalytic activity is a great tool as it is highly surface sensitive, i.e., even a thin $SiO_2$ layer on top of $TiO_2$ can prevent the generated electrons and holes to diffuse onto sample surface. Hence, the expectation would be that the samples with an increasing $SiO_2$ content will be photocatalytically less active in a linear manner than the pure $TiO_2$. Therefore, it is crucial to determine the photocatalytic activity as a function of $SiO_2/TiO_2$ ratio but keeping the average particle size almost constant.

Figure 2 shows the measured photocatalytic activity of the multicompound LFS nanoparticles deposited on a glass substrate. Two glasses were used in the reactor chamber to increase the active surface area for improved response from the $CO_2$ detector. Pure $TiO_2$ nanoparticle resulted in the highest photocatalytic activity with $CO_2$ increase of 26.2 ppm in 30 min. All multicompound $TiO_2/SiO_2$ samples showed a lower photocatalytic activity compared to the pure $TiO_2$ sample. Additionally, increase of $SiO_2$ content was followed by a lower $CO_2$ increase. With 5.0% $SiO_2$ content, no photocatalytic activity was observed. This is in contrary to our previous work [29], with multicompound nanoparticles used for controlled wettability on a paperboard in which up to 50% $SiO_2$ content was required to convert the initially superhydrophobic surface into a hydrophilic one.

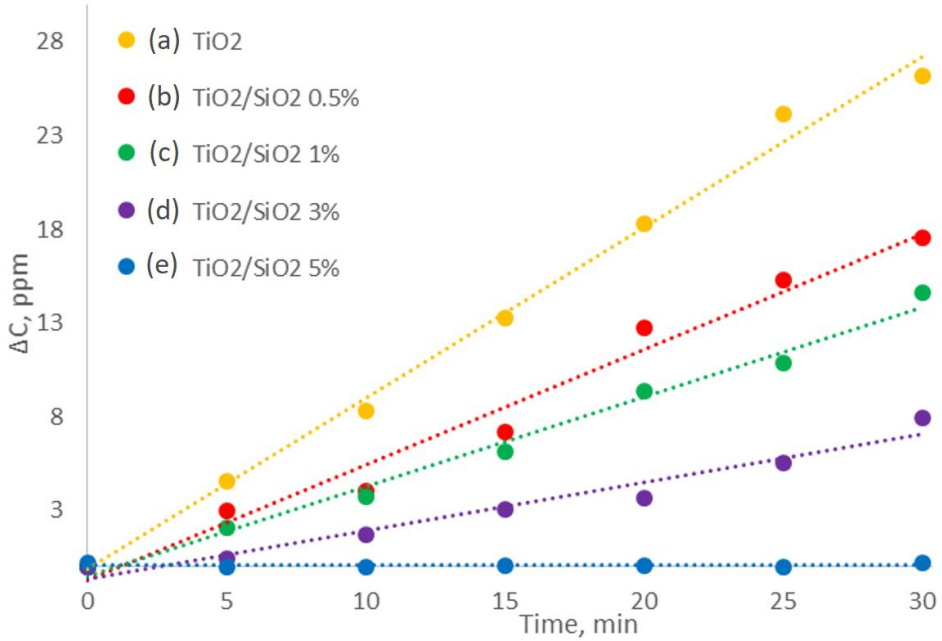


**Figure 2.** Measured photocatalytic activity of (**a**) $TiO_2$ 100% and $TiO_2/SiO_2$ multicompound nanoparticles with (**b**) $TiO_2/SiO_2$ 99.5/0.5, (**c**) $TiO_2/SiO_2$ 99.0/1.0, (**d**) $TiO_2/SiO_2$ 97.0/3.0 and (**e**) $TiO_2/SiO_2$ 95.0/5.0.

The rapid decrease of the photocatalytic activity by the increase of $SiO_2$ content may be associated with the LFS nanoparticle formation process in the flame during deposition. Both precursor solutions were fed into the same flame simultaneously and the nanoparticle formation process with two precursors is not well understood [30,31]. It is possible that $TiO_2$ nanoparticles nucleate first while $SiO_2$ nanoparticles nucleate later [32]. Hence, the first formed $TiO_2$ nanoparticles can provide a nucleation center for rapid covering layer of $SiO_2$. As a result, multicompound LFS deposition may produce a nanocomposite consisting of a $TiO_2/SiO_2$ core-shell structure. Furthermore, $SiO_2$ may also act as bridging agent between multicompound nanoparticles and between the substrate and the multicompound nanoparticles. The bandgap energy of $SiO_2$ is 8.9 eV (corresponding to 139 nm in the deep

UVC range) that requires significantly more energetic photons for photocatalytic excitation than anatase $TiO_2$ with a bandgap of 3.2 eV (387 nm) in the UVA range. The observed photocatalytic activity results support the hypothesis of a core-shell particle formation with even a thin $SiO_2$ layer on top of $TiO_2$ nanoparticles that can prevent the diffusion of the excited electron-hole pairs onto the surface.

For a more detailed characterization of the multicompound nanoparticles scanning transmission electron microscopy (STEM) was used with energy-dispersive X-ray (EDS) mapping. Figure 3 shows the STEM images with the corresponding EDS profiles of multicompound $TiO_2/SiO_2$ nanoparticles. Figure 3a shows STEM images of pure $TiO_2$ nanoparticles on microscope glass with average diameter of nanoparticles in range of 40–70 nm. Majority of nanoparticles have a spherical shape. The corresponding EDS profile verifies that nanoparticles consist of $TiO_2$ (characteristic peaks at 4.5 and 5.0 keV). Signals of copper and aluminum originate from the sample holder grid (characteristic peaks at 0.9 and 1.4 keV). No $SiO_2$ was observed as expected. Figure 3b,c display STEM images of $TiO_2/SiO_2$ 99.5/1.5 and 99.0/1.0 samples, respectively. No significant changes were observed in the nanoparticle morphology but the EDS profile indicated presence of $SiO_2$ characteristic peak (1.7 keV). Figure 3d shows the STEM image of $TiO_2/SiO_2$ 97.0/3.0. The size of nanoparticles was in the same range (40-70 nm) but the EDS profile showed an increase of Si content. Finally, Figure 3e presents the STEM image of $TiO_2/SiO_2$ 95.0/5.0. A small increase in the average diameter of nanoparticles (50–80 nm) was observed and the EDS profile displayed the highest amount of Si in all samples.

A tribology test with a cotton cloth square tip was performed to test adhesion of multicompound nanoparticles on glass substrate. The surfaces after tribological wear are presented on Figure 4 and show a more broken and smeared outlook with disordered nanoparticles. Agglomerated nanoparticles after tribological wear had a diameter of approximately 70–90 nm. Figure 4f shows the photographs of pure $TiO_2$ nanoparticle coated surface before and after tribological wear. The tribologically worn area is clearly seen in the center of image with photocatalytically active coating reduced approximately by 50%. Hence, the photocatalytic activity is expected to be reduced by a factor of two.

Figure 5 shows photocatalytic activity results of $TiO_2/SiO_2$ multicompound nanoparticles after tribological wear. As shown on Figure 4f, approximately 50% of the active area was tribologically worn. The removal of the active area roughly by half reduces the photoactivity in average by two as shown on Figure 5 with remaining activity ranging from 52.6% ($TiO_2$ sample) to 46.5% ($TiO_2/SiO_2$ 97.0/3.0). The highest rate of photo oxidation of $C_2H_2$ was observed with pure $TiO_2$ photocatalyst. As the content of $SiO_2$ was increased, the photocatalytic activity was decreased to 8.9 ppm, 6.6 ppm, 3.7 ppm and 0 ppm $SiO_2$ content of 0.5%, 1%, 3% and 5%, respectively.

The photocatalytic activation of $TiO_2$ is facilitated by absorption of a photon with energy equal to, or greater than, the band gap of $TiO_2$ (3.2 eV). This results in a generation of an electron–hole pair that can easily migrate onto the surface of the $TiO_2$ nanoparticle (Equation (1)). The surface water molecules react with oxygen in Ti-O-Ti bond and form a hydroxyl ion and a proton (See Equation (3)). Electrons formed upon absorption of light can react with absorbed oxygen generating highly reactive oxygen species (ROS, Equation (4)) whereas holes can interact with hydroxyl ion producing hydroxyl ion radical (Equation (5)). Hydroxyl ion radicals react with absorbed acetylene that is followed by photodegradation into $CO_2$ and $H_2O$ (Equation (6)). The overall reactions (1)–(6) are given below:

$$TiO_2 + h\nu \rightarrow TiO_2\ (e^-{}_{cb} + h^+{}_{vb}), \quad (1)$$

$$TiO_2\ (e^-{}_{cb} + h^+{}_{vb}) \rightarrow TiO_2{}^* + \text{heat} \quad (2)$$

$$TiO_2{}^* + H_2O_{ads} \rightarrow TiO_2 + OH^- + H^+ \quad (3)$$

$$e^-{}_{cb} + O_{2ads} \rightarrow O_2{}^- \quad (4)$$

$$h^+{}_{vb} + OH^- \rightarrow OH\bullet \quad (5)$$

$$2OH\bullet + C_2H_2 + 2O_2 \rightarrow 2CO_2 + 2H_2O \quad (6)$$

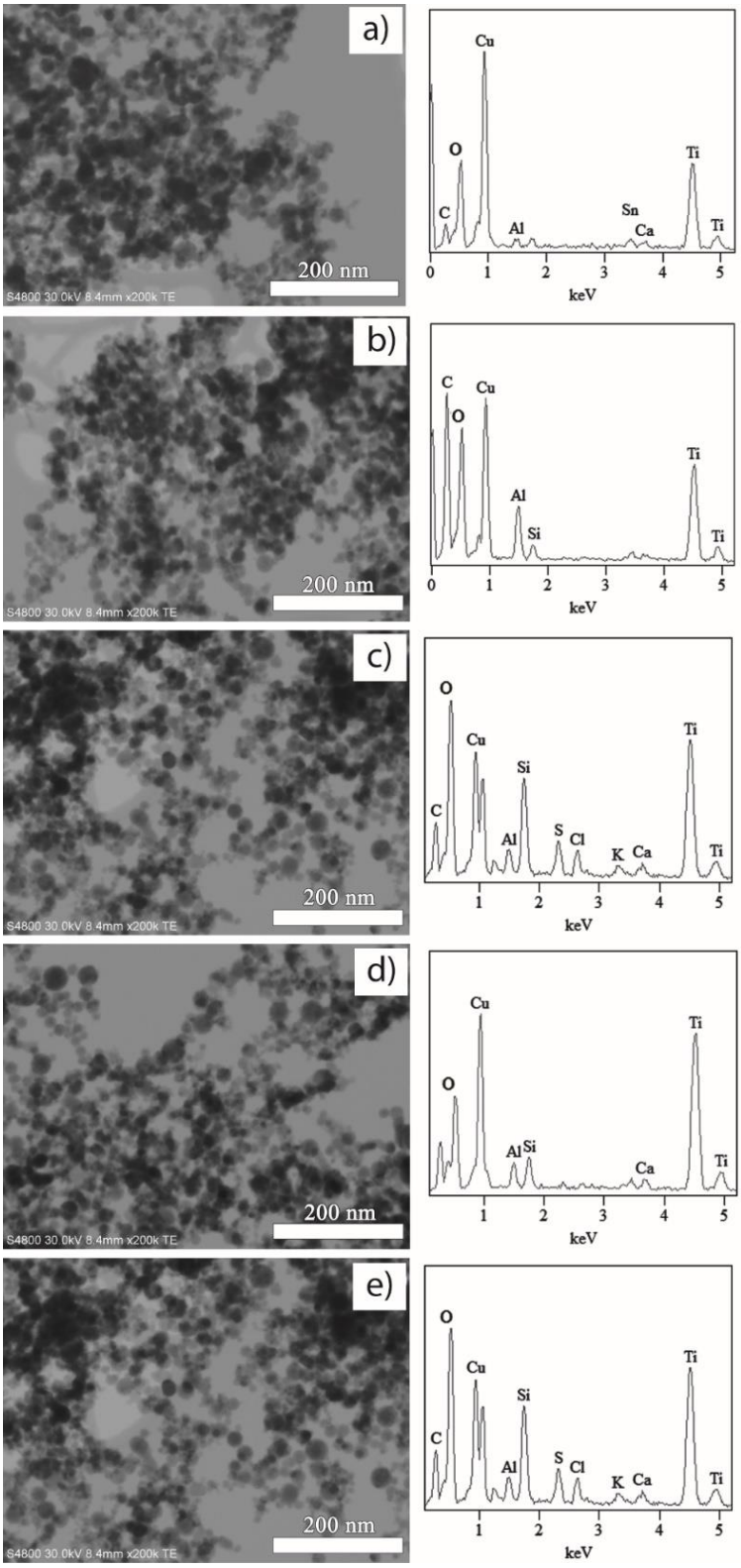


**Figure 3.** STEM images and EDS profiles of (**a**) $TiO_2$ 100%, (**b**) $TiO_2/SiO_2$ 99.5/0.5, (**c**) $TiO_2/SiO_2$ 99.0/1.0, (**d**) $TiO_2/SiO_2$ 97.0/3.0 and (**e**) $TiO_2/SiO_2$ 95.0/5.0).

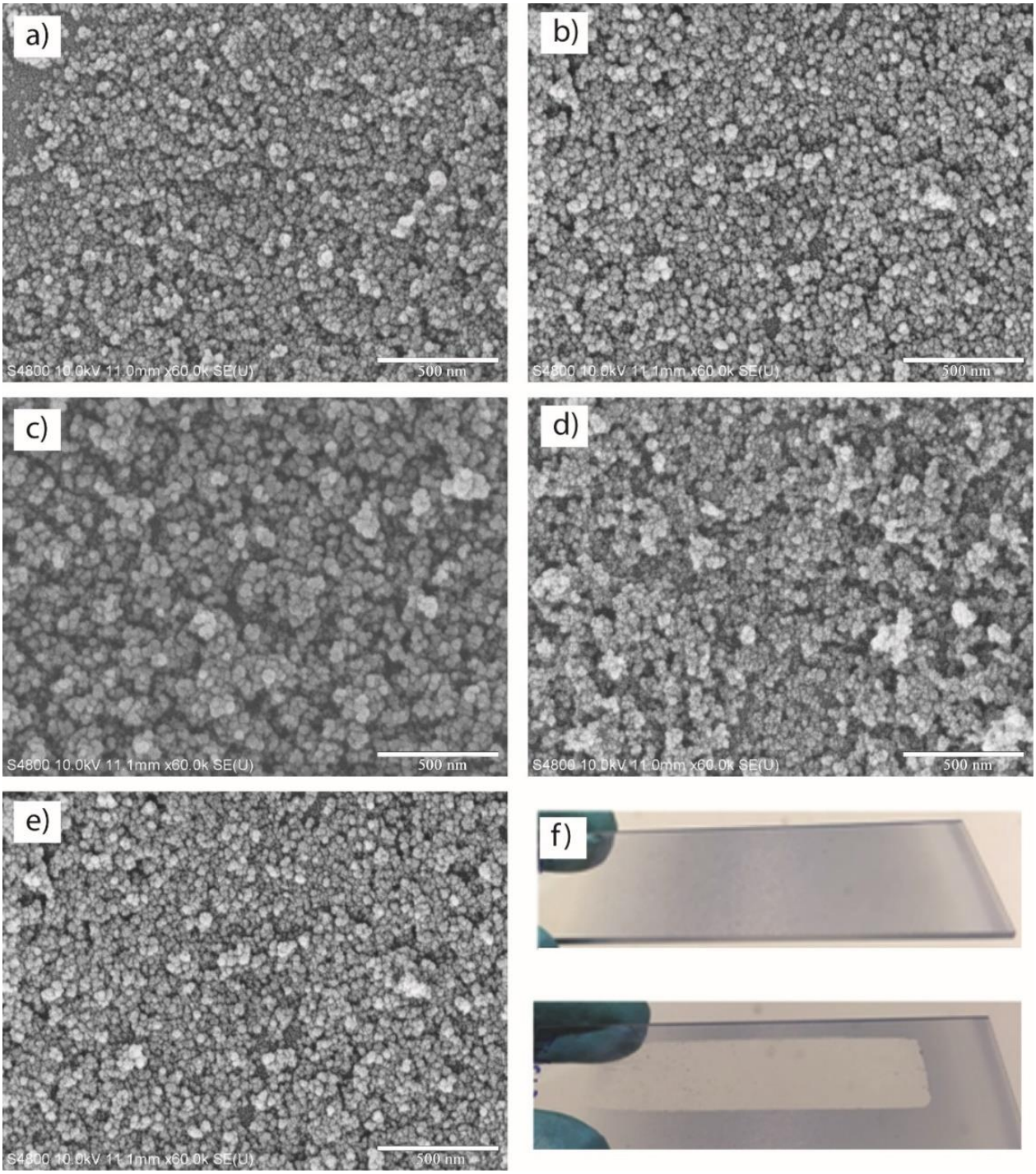


**Figure 4.** SEM images of (**a**) $TiO_2$, (**b**) $TiO_2/SiO_2$ 99.5/0.5, (**c**) $TiO_2/SiO_2$ 99.0/1.0, (**d**) $TiO_2/SiO_2$ 97.0/3.0 and (**e**) $TiO_2/SiO_2$ 95.0/5.0 after tribological wear. Photographs of the nanoparticle deposited microscope glass before and after the tribological wear are shown in (**f**).

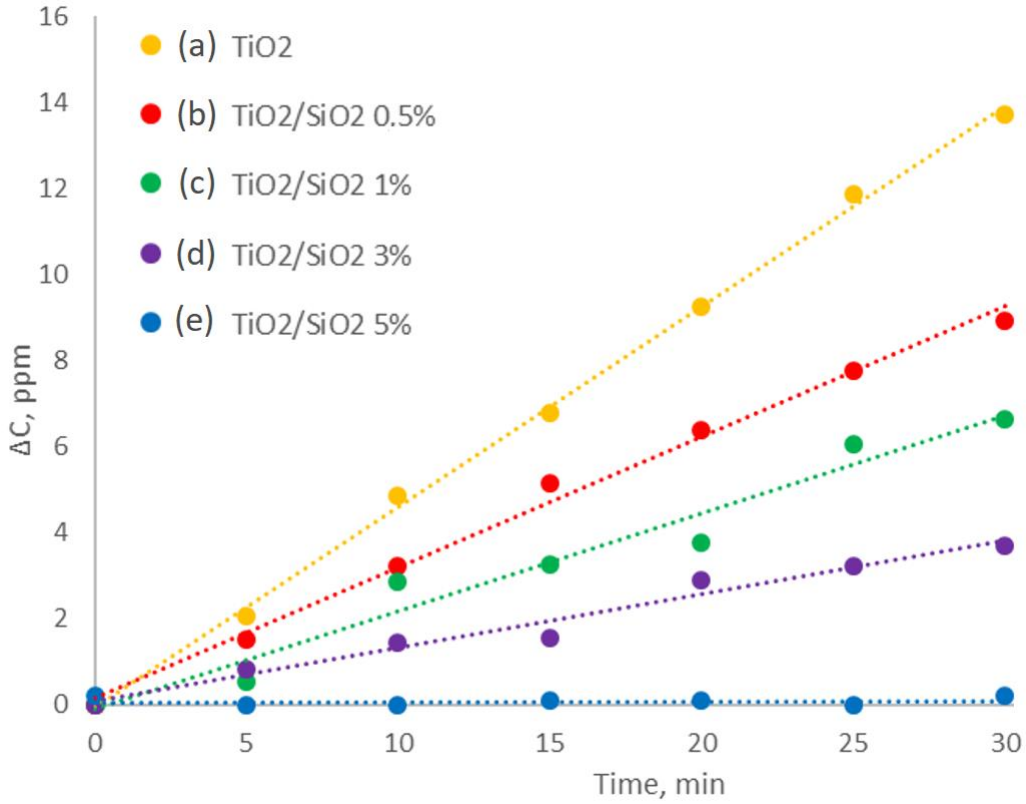


**Figure 5.** Measured photocatalytic activity of (**a**) $TiO_2$ 100% and $TiO_2/SiO_2$ multicompound nanoparticles with (**b**) $TiO_2/SiO_2$ 99.5/0.5, (**c**) $TiO_2/SiO_2$ 99.0/1.0, (**d**) $TiO_2/SiO_2$ 97.0/3.0 and (**e**) $TiO_2/SiO_2$ 95.0/5.0 after tribological wear.

The surface chemistry of the deposited multicompound nanoparticles was also characterized by water contact angle (WCA) measurements. Figure 6 shows the measured WCA values of the $TiO_2/SiO_2$ multicompound nanoparticles deposited on glass. For multicompound nanoparticles, the lowest value of 11.8° was observed with 0.5 silica content that was increased up to 34.1° with 5% $SiO_2$ content. These observations are in agreement with literature [33] of sol-gel deposited $TiO_2/SiO_2$ films that displayed a lower contact angle and increased photocatalytic degradation of MB with increased content of $TiO_2$ phase. The observed increase in the WCA supports the formation of a thin passivating $SiO_2$ layer on top of photocatalytically active $TiO_2$ particles. Capillary water absorption coefficients [34] can provide additional information about the wettability of multicompound nanoparticle coated surfaces and we plan to return to this issue in a future communication.

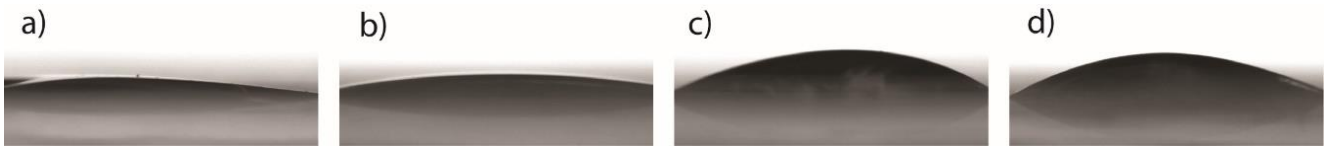


**Figure 6.** Water contact angle images of (**a**) $TiO_2/SiO_2$ 99.5/0.5, (**b**) $TiO_2/SiO_2$ 99.0/1.0, (**c**) $TiO_2/SiO_2$ 97.0/3.0 and (**d**) $TiO_2/SiO_2$ 95.0/5.0. 100% $TiO_2$ sample completely wetted the surface with WCA close to 0.

The observed results are in contrast to our previous work with wettability of multicompound $TiO_2/SiO_2$ nanoparticles on paperboard [29] that showed wettability conversion approximately at 50% $SiO_2$ increase, whereas here on glass even a 3% $SiO_2$ content resulted in a significant increase of the WCA. It is worth emphasizing here that our previous study was carried out on a paperboard in which the deposited nanoparticles collect volatile hydrocarbons evaporated from the deposited paperboard substrate. On paperboard the wettability formed an S-shaped curve as a function of the $TiO_2$ fraction (in fact, the ratio of

Ti/(Si + Ti) content in the used precursor for LFS) when scanned through all the $SiO_2/TiO_2$ compositions. This meant that 0% and 10% of $TiO_2$ deposits collected the least amount of hydrocarbons, whereas 90% and 100% of $TiO_2$ deposits collect the most hydrocarbons. This was followed by the observed S-curve behavior from highly wetting state to highly non-wetting state around 50% $TiO_2$ content. In this study, no volatile organic compounds were present as glass was used as a substrate.

## 3. Materials and Methods

### *3.1. Liquid Flame Spray (LFS) Multicompound Nanoparticle Deposition*

Functional multicompound nanoparticles were generated using a liquid flame spray (LFS) nanoparticle deposition that allows a cost-efficient deposition of various metal and metal oxide nanoparticles in atmospheric conditions for large areas [17,18] as shown schematically on Figure 7a. LFS contains a high temperature and a high velocity flame in which an organometallic precursor evaporates, nucleates and forms solid nanoparticles of the final material. LFS multicompound nanoparticle deposition was carried out using single nozzle type burner and the microscope glass samples were attached in a rotating carousel for the nanoparticle deposition. The nozzle was placed 6 cm away from the sample surface. Hydrogen and oxygen were used for the combustion gases with gas flow rates of 50 L/min and 15 L/min, respectively. The precursor feed rate was set to 12 mL/min. As the combined total concentration of titanium and silicon was fixed to 50 mg/mL, this resulted in production rate of 600 mg of $TiO_2/SiO_2$ nanoparticles in minute. Ratio of Si was varied between 0 and 5% and a total of 5 different $TiO_2/SiO_2$ ratios were used.

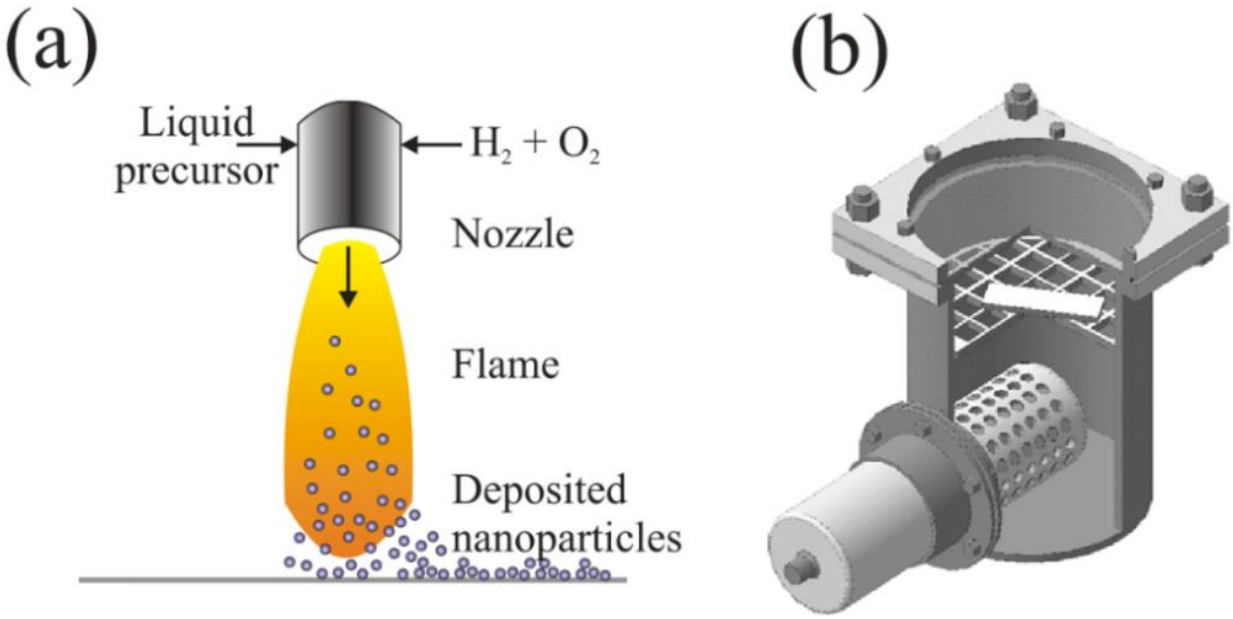


**Figure 7.** Schematic picture of (**a**) LFS nanoparticle deposition and (**b**) the used gas-phase detector for photocatalytic activity characterization.

### *3.2. Photocatalytic Activity Characterization by Gas-Phase Oxidation of Acetylene*

An in-house built gas-phase reactor for photocatalytic activity characterization was constructed from stainless steel with a shell diameter of 145 mm and volume of 15.4 $cm^3$ as shown on Figure 7b. A removable lid consists of UV transparent glass and flange connection with reactor shell. The reactor was equipped with $CO_2$ detector (Vaisala GMP343, Vantaa, FI), temperature and humidity sensor (Thorlabs TSP01, Newton, NJ, US) and pressure meter (Wika PGT10, USB mode, Klingenberg, DE). All detectors were USB connected to the PC for a real-time measurement [27,28].

The photocatalytic activity measurement was carried out using acetylene ($C_2H_2$) and technical air that were supplied to the mixing chamber. The technical air played a role as a carrier of acetylene to the reaction chamber and proportion of technical air to acetylene was set to 3:1. Only gas-phase constituents were utilized in photocatalytic activity detection and there is no need for a buffer solution in gas-phase detection in contrast to cyclic voltammetry. The gases flow inside the reactor was continuous until the $CO_2$ concentration becomes constant. Once the concentration of $CO_2$ was stabilized, the valves were shut down and the concentration increase of photogenerated $CO_2$ was monitored (a batch type reactor). The ultraviolet A (UVA) lamp (UVP Black-Ray® B-100AP High Intensity, Cambridge, UK, 100 W) with peak emission at 365 nm and intensity of approximately 20 mW/cm$^2$ was located 17 cm above the reactor lid.

The detection method is based on oxidation of acetylene into $CO_2$ and $H_2O$. The main parameters of the photocatalytical reaction such as pressure and humidity during photocatalytical reaction did not change significantly and were assumed to be constant (40–50% and atmospheric pressure). An external ventilation was applied to remove excess heat from the UVA lamp and the overall temperature was kept in the range of 27–30 °C. After completion of the measurement, the valves can be opened and the reactor can be filled with technical air to remove all reaction components before the subsequent measurements. All photocatalytic activity results are an average of three, almost overlapping, parallel measurements that verifies the stability and reproducibility of both the used measurement system and the multicompound photocatalysts with no mechanical stresses induced on the nanostructured surface during the gas-phase detection.

### *3.3. Tribological Wear of the Nanoparticle Coated Microscope Glasses*

Tribological wear test was performed using a tribometer (CSM+ Instruments Tribometer TRN S/N 18-347, Needham, MA, USA). The tribometer with a square tip (area of $1 \times 1$ cm$^2$) covered with a cotton layer by double-side tape was used with two cycles with a 3 N force during 10 s. The tribologically worn area was approximately 50% of the deposited nanoparticle area as displayed on Figure 4. The friction data was collected with a ModelIX software (CSM+ Instruments, Needham, MA, USA).

### *3.4. Scanning and Scanning Transmission Electron Microscope (SEM/STEM) Imaging*

The morphology and average structural sizes of $TiO_2$ nanoparticles were observed with Hitachi S-4800 FE-SEM (field emission scanning electron microscope, Tokyo, Japan). Scanning electron microscope (SEM) images were acquired after cutting microscope slide to small squares ($2 \times 2$ cm$^2$).

### *3.5. Absorption Spectrum*

A PerkinElmer Lambda 900 UV−vis/NIR spectrometer (Waltham, MA, USA) with a 150 mm integrating sphere was used to measure the absorption spectra of the multicompound nanoparticles.

### *3.6. Wettability Characterization*

Water contact angle (WCA) measurements were carried out using a KSV Cam 200 (KSV Instruments Ltd., Helsinki, Finland) contact angle goniometer with 4 μL deionized water droplet at a room temperature. A Young–Laplacian fitting protocol was utilized to calculate the WCA value from the measured droplet profile.

## 4. Conclusions

We investigated LFS deposited $TiO_2/SiO_2$ multicompound nanoparticles for photocatalytic activity. The addition of $SiO_2$ content did not improve nanoparticle adhesion but significantly reduced the photocatalytic activity, with the $TiO_2/SiO_2$ 95.0/5.0 sample showing no photocatalytic activity. During a simultaneous deposition in the LFS flame, $SiO_2$ was probably deposited on top of $TiO_2$ nanoparticles, followed by significantly reduced

photocatalytic activity. The deposition of $SiO_2$ on top of $TiO_2$ was also supported by the changes in the surface wettability.

Our future studies will involve multicompound metal (Ag or Au) combined with photocatalytic metal oxide ($TiO_2$ or ZnO) nanoparticles in which even a visible light can activate the photocatalysis via plasmonic activation of the metallic nanomaterials. For improved adhesion of $TiO_2$ nanoparticles on glass surface, a precursor layer will be studied. We believe that multicompound nanomaterials will find many applications in solar-driven photocatalysis and chemistry in future.

**Author Contributions:** F.T. carried out the photocatalytic measurements, data analysis and wrote the first draft of the manuscript. J.H. performed the LFS nanoparticle depositions. J.M.M. supervised the LFS nanoparticle depositions. J.J.S. coordinated the joint research and finalized the manuscript. All authors have read and agreed to the published version of the manuscript.

**Funding:** This research was funded by Finnish Cultural Foundation for a research grant to F.T. J.J.S. acknowledges the Faculty of Science and Forestry at the University of Eastern Finland for the financial support (grant no. 579/2017) and the Academy of Finland Flagship for Photonics Research and Innovation (PREIN, decision no. 320166).

**Institutional Review Board Statement:** Not applicable.

**Informed Consent Statement:** Not applicable.

**Data Availability Statement:** The data presented in this study are available in article here. The data presented in this study are also available on request from the corresponding author.

**Conflicts of Interest:** The authors declare no conflict of interest.

## References

1. Nickheslat, A.; Amin, M.M.; Izanloo, H.; Fatehizadeh, A.; Mousavi, S.M. Phenol Photocatalytic Degradation by Advanced Oxidation Process under Ultraviolet Radiation Using Titanium Dioxide. *J. Environ. Res. Public Health* **2013**, *2013*, 1–9. [CrossRef] [PubMed]
2. Zaleska-Medynska, A.; Gołąbiewska, A.; Kobylański, M.P. Metal Oxide-Based Photocatalysis. Fundamentals and Prospects for Application. In *Metal Oxide-Based Photocatalysis*; Korotcenkov, G., Ed.; Elsevier: Amsterdam, The Netherlands, 2018; pp. 3–50.
3. Schneider, J.; Matsuoka, M.; Takeuchi, M.; Zhang, J.; Horiuchi, Y.; Anpo, M.; Bahnemann, D.W. Understanding $TiO_2$ Photocatalysis: Mechanisms and Materials. *Chem. Rev.* **2014**, *114*, 9919–9986. [CrossRef]
4. Fujishima, A.; Honda, K. Electrochemical Photolysis of Water at a Semiconductor Electrode. *Nature* **1972**, *238*, 37. [CrossRef]
5. Ran, J.; Jaroniec, M.; Qiao, S.-Z. Cocatalysts in semiconductor-based photocatalytic $CO_2$ reduction: Achievements, challenges, and opportunities. *Adv. Mater.* **2018**, *30*, 1704649. [CrossRef]
6. Chen, X.; Shen, S.; Guo, L.; Mao, S.S. Semiconductor-based photocatalytic hydrogen generation. *Chem. Rev.* **2010**, *110*, 6503–6570. [CrossRef]
7. Karapati, S.; Giannakopoulou, T.; Todorova, N.; Boukos, N.; Dimotikali, D.; Trapalis, C. Eco-efficient $TiO_2$ modification for air pollutants oxidation. *Appl. Catal. B Environ.* **2015**, *176*, 578–585. [CrossRef]
8. Khairy, M.; Zakaria, W. Effect of metal-doping of $TiO_2$ nanoparticles on their photocatalytic activities toward removal of organic dyes. *Egypt. J. Pet.* **2014**, *23*, 419–426. [CrossRef]
9. Yalç, Y.; Murat, K.; Zekiye, Ç. The Role of Non-Metal Doping in $TiO_2$ Photocatalysis. *J. Adv. Oxid. Technol* **2010**, *13*, 281–296.
10. Quesada, J.; Arreola-Sánchez, R.; Faba, L.; Díaz, E.; Rentería-Tapia, V.M.; Ordóñez, S. General Effect of Au nanoparticles on the activity of $TiO_2$ for ethanol upgrading reactions. *Appl. Catal. A* **2018**, *551*, 23–33. [CrossRef]
11. Ismail, A.A.; Abdelfattah, I.; Faycal Atitar, M.; Robben, L.; Bouzid, H.; Al-Sayari, S.A.; Bahnemann, D.W. Photocatalytic degradation of imazapyr using mesoporous $Al_2O_3$–$TiO_2$ nanocomposites. *Separ. Purif. Technol.* **2015**, *145*, 147–153. [CrossRef]
12. Setthaya, N.; Chindaprasirt, P.; Yin, S.; Pimraksa, K. $TiO_2$-zeolite photocatalysts made of metakaolin and rice husk ash for removal of methylene blue dye. *Powder Technol.* **2017**, *313*, 417–426. [CrossRef]
13. Gao, J.; Li, W.; Zhao, X.; Wang, L.; Pan, N. Durable visible light self-cleaning surfaces imparted by $TiO_2/SiO_2$/GO photocatalyst. *Textile Res. J.* **2019**, *89*, 517–527. [CrossRef]
14. Nabih, S.; Esmail Shalan, A.; Samy Abu Serea, E.; Goda, M.A.; Fathi Sanad, M. Photocatalytic performance of $TiO_2$@$SiO_2$ nanocomposites for the treatment of different organic dyes. *J. Mat. Sci. Mater. Electron.* **2019**, *30*, 9623–9633. [CrossRef]
15. Bellardita, M.; Addamo, M.; Di Paola, A.; Marcì, G.; Palmisano, L.; Cassar, L.; Borsa, M. Photocatalytic activity of $TiO_2/SiO_2$ systems. *J. Hazard. Mater.* **2010**, *174*, 707–713. [CrossRef]
16. Xu, L.; Shen, Y.; Ding, Y.; Wang, L. Superhydrophobic and ultraviolet-blocking cotton fabrics based on $TiO_2/SiO_2$ composite. Nanopart. *J. Nanosc. Nanotechnol.* **2018**, *18*, 6879–6886. [CrossRef] [PubMed]

17. Mäkelä, J.M.; Aromaa, M.; Teisala, H.; Tuominen, M.; Stepien, M.; Saarinen, J.J.; Toivakka, M.; Kuusipalo, J. Nanoparticle Deposition from Liquid Flame Spray onto Moving Roll-to-Roll Paperboard Material. *J. Aerosol Sci.* **2011**, *68*, 827–837. [CrossRef]
18. Mäkelä, J.M.; Haapanen, J.; Harra, J.; Juuti, P.; Kujanpää, S. Liquid Flame Spray—A Hydrogen-Oxygen Flame Based Method for Nanoparticle Synthesis and Functional Nanocoatings. *KONA Powder Part. J.* **2017**, *34*, 141–154. [CrossRef]
19. Mädler, L.; Roessler, A.; Pratsinis, S.E. Direct formation of highly porous gas-sensing films by in situ thermophoretic deposition of flame-made Pt/$SnO_2$ nanoparticles. *Sens. Actuators B Chem.* **2006**, *114*, 283–295. [CrossRef]
20. Stepien, M.; Saarinen, J.J.; Teisala, H.; Tuominen, M.; Aromaa, M.; Kuusipalo, J.; Mäkelä, J.M.; Toivakka, M. Adjustable wettability of paperboard by liquid flame spray nanoparticle deposition. *Appl. Surf. Sci.* **2011**, *257*, 1911–1917. [CrossRef]
21. Stepien, M.; Saarinen, J.J.; Teisala, H.; Tuominen, M.; Aromaa, M.; Kuusipalo, J.; Mäkelä, J.M.; Toivakka, M. Surface chemical analysis of photocatalytic wettability conversion of $TiO_2$ nanoparticle coating. *Surf. Coat. Technol.* **2012**, *208*, 73–79. [CrossRef]
22. Stepien, M.; Saarinen, J.J.; Teisala, H.; Tuominen, M.; Aromaa, M.; Haapanen, J.; Kuusipalo, J.; Mäkelä, J.M.; Toivakka, M. ToF-SIMS analysis of UV-switchable $TiO_2$-nanoparticle coated paper surface. *Langmuir* **2013**, *29*, 3780–3790. [CrossRef]
23. Stepien, M.; Saarinen, J.J.; Teisala, H.; Tuominen, M.; Haapanen, J.; Kuusipalo, J.; Mäkelä, J.M.; Toivakka, M. Compressibility of porous $TiO_2$ nanoparticle coating on paperboard. *Nanoscale Res. Lett.* **2013**, *8*, 1–6. [CrossRef] [PubMed]
24. Teisala, H.; Geyer, F.; Haapanen, J.; Juuti, P.; Mäkelä, J.M.; Vollmer, D.; Butt, H.J. Ultrafast processing of hierarchical nanotexture for a transparent superamphiphobic coating with extremely low roll-off angle and high impalement pressure. *Adv. Mater.* **2018**, *30*, 1706529. [CrossRef] [PubMed]
25. Xu, C.; Rangaiah, G.P.; Zhao, X.S. Photocatalytic degradation of methylene blue by titanium dioxide: Experimental and modeling study. *Ind. Eng. Chem. Res.* **2014**, *53*, 14641–14649. [CrossRef]
26. Yan, X.; Ohno, T.; Nishijima, K.; Abe, R.; Ohtani, B. Is methylene blue an appropriate substrate for a photocatalytic activity test? A study with visible-light responsive titania. *Chem. Phys. Lett.* **2006**, *429*, 606–610. [CrossRef]
27. Temerov, F.; Ankudze, B.; Saarinen, J.J. $TiO_2$ inverse opal structures with facile decoration of precious metal nanoparticles for enhanced photocatalytic activity. *Mater. Chem. Phys.* **2020**, *242*, 122471. [CrossRef]
28. Pham, K.; Temerov, F.; Saarinen, J.J. Multicompound inverse opal structures with gold nanoparticles for visible light photocatalytic activity. *Mater. Des.* **2020**, *194*, 108886. [CrossRef]
29. Haapanen, J.; Aromaa, M.; Teisala, H.; Tuominen, M.; Stepien, M.; Saarinen, J.J.; Heikkilä, M.; Toivakka, M.; Kuusipalo, J.; Mäkelä, J.M. Binary $TiO_2/SiO_2$ nanoparticle coating for controlling the wetting properties of paperboard. *Mater. Chem. Phys.* **2015**, *150*, 230–237. [CrossRef]
30. Keskinen, H.; Mäkelä, J.M.; Aromaa, M.; Ristimäki, J.; Kanerva, T.; Levänen, E. Effect of silver addition on the formation and deposition of titania nanoparticles produced by liquid flame spray. *J. Nanopart. Res.* **2007**, *9*, 569–588. [CrossRef]
31. Ulrich, G.D. Theory of Particle Formation and Growth in Oxide Synthesis Flames. *Combust. Sci. Technol.* **1971**, *4*, 47–57. [CrossRef]
32. Teleki, A.; Pratsinis, S.E.; Wegner, K.; Jossen, R. Flame-coating of titania particles with silica. *J. Mater. Res.* **2005**, *20*, 1336–1347. [CrossRef]
33. Kwon, C.H.; Kim, J.H.; Jung, I.S.; Shin, H.; Yoon, K.H. Preparation and characterization of $TiO_2$–$SiO_2$ nano-composite thin films. *Cer. Int.* **2003**, *29*, 851–856. [CrossRef]
34. Kapridaki, C.; Maravelaki-Kalaitzaki, P. $TiO_2$–$SiO_2$–PDMS nano-composite hydrophobic coating with self-cleaning properties for marble protection. *Prog. Org. Coat.* **2013**, *76*, 400–410. [CrossRef]